#### **CAAP Quarterly Report**

### [09/25/2025]

Project Name: "All-in-One Multifunctional Cured-In-Place Structural Liner for Rehabilitating of Aging Cast Iron Pipelines"

Contract Number: 693JK32250009CAAP

Prime University: North Dakota State University

Prepared By: [Ying Huang, ying.huang@ndsu.edu, 701-231-7651]

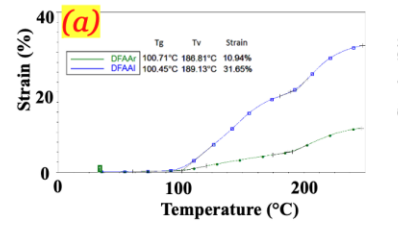
Reporting Period: [06/27/2025-09/27/2025]

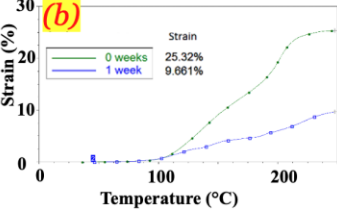
## **Project Activities for Reporting Period:**

In the 11<sup>th</sup> quarterly report, Tasks 2, 3, 4, and 5 were carried out as proposed. During the current reporting period (Q12), the research team continued to make steady progress on these tasks. Key accomplishments from this quarter are summarized in the sections that follow.

Task 2.1 Preparation of Vitrimer Epoxy Resins, Characterization, and Optimization of Processing and Curing Conditions (99%): During the past quarter, the research team (Dr. Long Jiang and Austin Knight, Ph.D. student at NDSU), investigated new formulation strategies using an acrylate reactive diluent containing a significant amount of diacrylate impurities. This modified formulation was designed to enhance thermal properties. This quarter, the team evaluated the properties of formulations incorporating this short chain aliphatic crosslinker (DFAAl). In addition, longer-chain aliphatic crosslinkers (referred to as DFAAl2 and DFAAl3) were synthesized to explore further improvements in performance. Key findings from these efforts are summarized below:

(1) Formulation Aging after Adding on Short Chain Aliphatic Crosslinker (DFAAl): In the previous quarter, a short-chain aliphatic crosslinker (DFAAl) was synthesized. Formulations containing DFAAl with 100 parts methacrylate reactive diluent (RDMA) and 20 parts transesterification catalyst (TEC) exhibited higher strain above the glass transition temperature (Tg) and topology freezing temperature (Tv) than those with aromatic crosslinkers (Figure D-1(a)). This increased strain suggested better flow at elevated temperatures, potentially enhancing the material's self-healing capability. However, retesting showed that results with DFAAl were not reproducible. After preparing a new batch, it was found that aging of the formulation, after mixing RDMA, TEC, and photoinitiator (PI) with the crosslinker, was responsible. When stored for a week, the final strain during dilatometry testing dropped significantly (Figure 1(b)). Therefore, all subsequent tests were conducted immediately after mixing.





results at 100kPa for formulations containing 100-RDMA and 20-TEC, (a) DFAAr and DFAAl and (b) DFAAl tested immediately and after one week.

(2) FTIR of DFAAl: The short-chain crosslinkers were synthesized, forming hydroxyester linkages via the reaction of carboxylic acid and epoxide groups. FTIR spectra of the reagents and the DFAAl 10-RDMA mixture, before and after heating at 90 °C for 24 hours, are shown in Figure D-2. The

reduction of peaks at 1615 and 1432 cm<sup>-1</sup> indicates consumption of the conjugated C=C stretch and O-H bending from acrylic acid. A new peak at 1406 cm<sup>-1</sup> corresponds to the formation of hydroxyl groups in the hydroxyester. The disappearance of peaks at 844 and 759 cm<sup>-1</sup> confirms the complete conversion of epoxide groups. These results confirm that the expected reaction occurred, with excess acrylic acid remaining, which is preferred over residual epoxy since the acrylic acid can still participate in UV-curing polymerization.

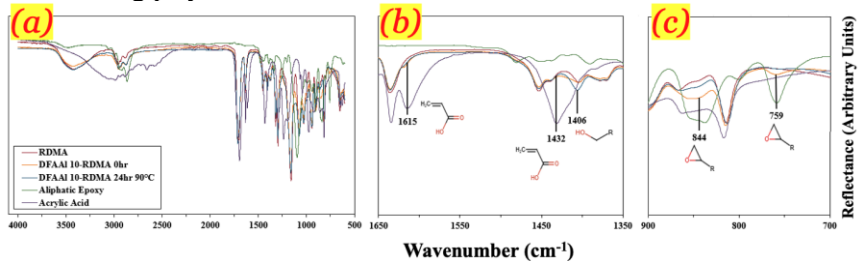


**Figure D-2.** The (a) full, (b) 1650-1350 cm<sup>-1</sup>, and (c) 900-700 cm<sup>-1</sup> FTIR spectra for RDMA, DFAAl 10-RDMA before heating, DFAAl 10-RDMA after heating at 90°C for 24 hours.

(3) Hydroxyl Containing Solvent for the TEC: It was found that the TEC powder did not disperse well in the resin, often settling out and causing inconsistencies in catalyst content. Larger undissolved particles also cured into the adhesive, introducing stress concentration points. To improve homogeneity, the best-performing hydroxyl-containing solvent (HS) from previous evaluations was used to dissolve the TEC. However, dissolving 20 parts TEC required so much HS that the resin remained too soft after curing. Similarly, formulations with 5 parts TEC and sufficient HS were also too soft. A 1-part TEC formulation with 10 parts HS maintained adequate rigidity for testing. To further improve mechanical strength, crosslinker content was increased (Figure D-3(a)), but no observable topology freezing temperature (Tv) was detected, suggesting that the TEC concentration was still too low for vitrimer behavior. Additional trials used higher TEC content with only enough HS to aid dispersion, not full dissolution. Formulations like 20-TEC 20-HS and 10-TEC 10-HS formed unworkable pastes and cured into soft, uncrosslinked samples. A 5-TEC 5-HS formulation was rigid at room temperature and tested against the same without HS (Figure 3(b)). The HS-containing formulation showed significantly higher strain, requiring the applied stress to be reduced from 100 kPa to 50 kPa to avoid exceeding the DMA's motion range. While HS improves TEC dispersion and increases final strain, it also lowers Tg and Tv. Therefore, its content must be carefully balanced to prevent excessive softening of the cured adhesive.

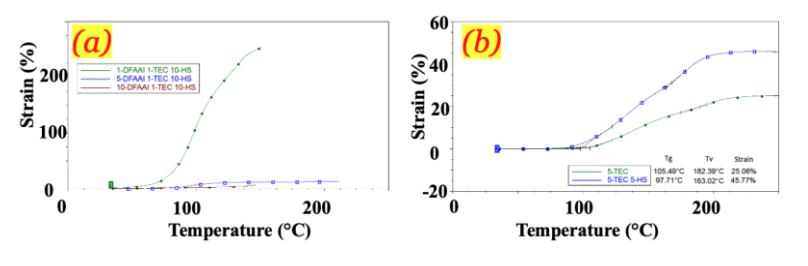


Figure D-3. Dilatometry results of formulations containing 100-RDMA and 20-TEC and (a) 1, 5, and 10-DFAAl, 1-TEC, and 10-HS at 100kPa and (b) DFAAl, 5-TEC, and 0 and 5-HS at 50kPa.

Task 3.3 Reducing the Permeability and Investigating the Interfacial Bonding Chemical Analysis (90%): In previous work, the research team (Dr. Liangliang Huang and Hao Yuan, Ph.D. student at the University of Oklahoma) performed a comprehensive evaluation of the previously developed vitrimer model was carried out. During this reporting period, the vitrimer system was scaled up to achieve a more representative cluster size distribution. Based on this larger system, previously reported properties, including glass transition temperature, porosity, and mechanical performance, were re-evaluated. Additionally, the cluster size distribution of polymer chains within the vitrimer network were further analyzed.

- (1) Cluster Size Distribution: Vitrimer systems modeled via chain-growth polymerization achieved a high extent of reaction ( $\xi > 99\%$ ) within 5 ns of simulation. As shown in Figure D-5, the resulting cluster size distribution is heavily skewed toward smaller aggregates, with most polymers
  - containing fewer than 150 atoms, particularly concentrated in the 0–50 atom range. This distribution stems from the nature of chain-growth polymerization, where early reactions occur primarily between monomers or monomers and short oligomers. As the reaction proceeds and monomer concentration drops, reactive site availability declines, limiting the formation of high-molecular-weight species and

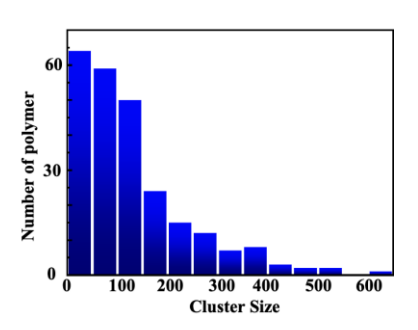


Figure D-5. Distribution of cluster size for final chaingrowth configurations.

maintaining the bias toward smaller clusters even at high conversion.

(2) Thermal Expansion Coefficient: The glass transition temperature (Tg) of the enlarged system was calculated using the same method as in the previous study. The result, 399 K (Figure D-6), is slightly higher than before and aligns more closely with experimental data. Tg was identified as the intersection point of fitted lines in the glassy and rubbery regions of the specific volume—temperature curve. The thermal expansion coefficient (α), which increases with temperature, also helps distinguish these regimes. In the glassy region (200–300 K), α remains low due to restricted molecular mobility. Around 400 K, α rises sharply, marking the onset of Tg, and stabilizes near 450 K, indicating the system's full transition into the rubbery state.

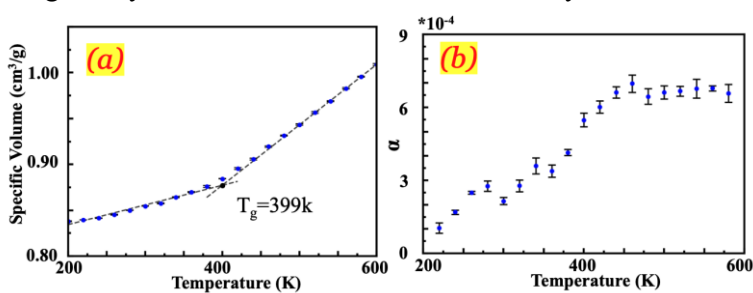


Figure D-6. (a) Specific volume and (b) thermal expansion coefficient as a function of temperature.

(3) Mechanical Property: The stress-strain behavior of the polymer is significantly influenced by temperature (Figure D-7). As temperature increases, both thermoset and vitrimer systems exhibit

thermal softening, as evidenced by a reduction in stiffness. At 300 K, the mechanical properties of the vitrimer are nearly identical to

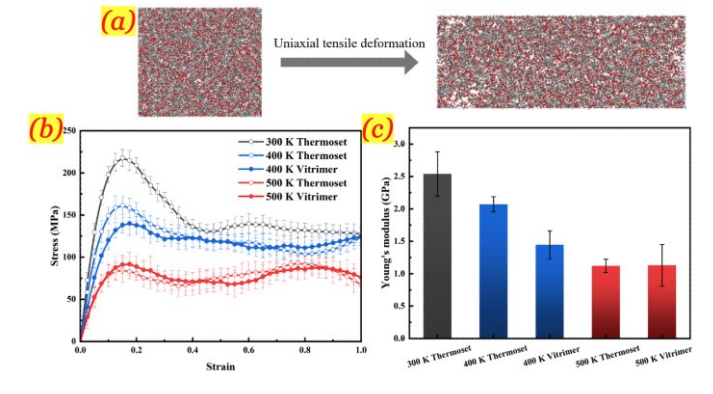


Figure D-7. (a)
Tensile deformation
schematic diagram.
(b) Stress-strain
curves of thermosets
and vitrimers and (c)
corresponding
Young's modulus.

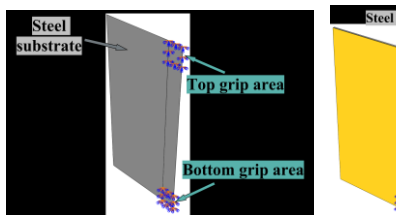
those of the thermoset, with a calculated Young's modulus of approximately 2.5 GPa. At 400 K, the onset of bond exchange reactions leads to a noticeable reduction in the Young's modulus of the vitrimer compared to the thermoset, indicating that these dynamic reactions weaken the material's

resistance to deformation. However, at 500 K, the modulus values of both systems converge. This convergence is attributed to the fact that the materials have transitioned into a melt-like state, where polymer chain mobility dominates the mechanical response, and the influence of bond exchange reactions becomes negligible.

Task 3.4 Finite Element Numerical Analysis to Guide the Design of the Developed High-performance Healable CIPP Structural Liner (96%): During this reporting period, the research team (Dr. Chengcheng Tao, Junyi Duan and Yizhou Lin, Ph.D. students from Purdue University) have conducted finite element analysis (FEA) on investigating the response of pipe-liner system subjected to eccentric compression, dent and corrosion defects as summarized below:

(1) Finite Element Model of the Pipe-Liner System Subjected to Buckling: To simulate the mechanical behavior of the test samples under eccentric compressive load, finite element analysis (FEA) is performed. Two finite element models are developed to represent the experimental conditions. Figure D-8 exhibits the finite element models of the single steel substrate and the CIPP-liner rehabilitated steel substrate. The single steel substrate is modeled using shell elements (S4R). The

developed finite element model simulates the CIPP liner-rehabilitated steel substrate, which includes three layers: the steel substrate, an adhesive layer, and a



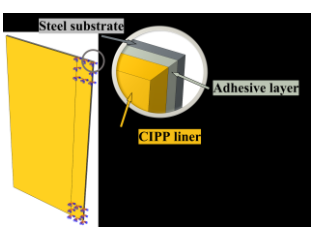


Figure D-8.
The FEA
models of
(a) steel and
(b) linerprotected
steel.

fiber-reinforced polymer CIPP liner. The interfacial property is simplified as the tied constraint. The top corner is constrained to rotation and only allowed to move vertically by 7 mm. Initial imperfections are introduced into the model to reflect the structural irregularities in practice.

(2) Analysis of Pipe-Liner System Subjected to Buckling: By correlating strain fields from DFOS and FEA, the mechanical response of the liner-rehabilitated steel substrate is extracted through simulation. The digital twin framework capturing this deformation is shown in Figure D-9. To enhance its functionality, damage information is overlaid: red irregular regions indicate damage at

the adhesive-steel interface, while yellow regions show damage at the adhesive-liner interface. Larger areas suggest more severe damage. Notably, more damage occurs at the steel interface, underscoring the need

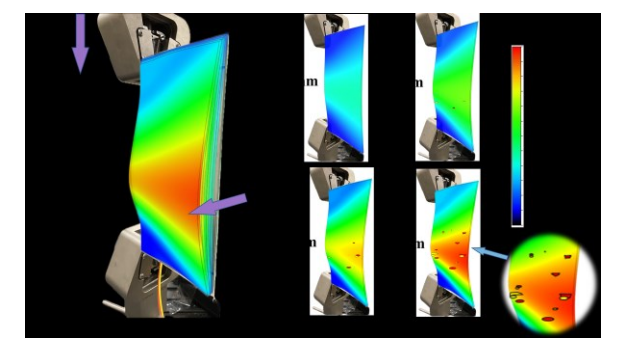
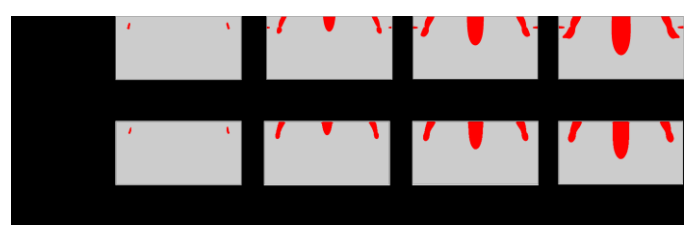


Figure D-9. The developed 3D damage-informed digital-twin framework for deformation visualization of liner-rehabilitated steel substrate.

for strong adhesion in rehabilitation. Although less damage is seen at the liner interface, it appears earlier, highlighting the value of DFOS-integrated liners for early detection. The strain on the adhesive-layer-steel interface is estimated theoretically based on the strain results obtained from adhesive layer-liner interface. Based on the estimated strain in the steel substrate, the structural condition of the entire substrate can be predicted. Figure D-10 shows the comparison between the estimated plastic regions from the FEA and the theoretically predicted plastic regions in the steel layer. The prediction results align well with the FEA results, with minor differences observed near the edge of the grip areas. Moreover, the plastic deformation initiates near the grip areas and

propagates toward high deformation regions. The results demonstrate that the integrating DFOS with the liner enables reliable prediction of the strain-based condition of the steel substrate. This approach shows strong potential for the application in the underground pipe industry for structural health monitoring purpose.



**Figure D-10.** Comparison of plastic regions of the steel layer of liner-rehabilitated steel substrate at displacement levels.

**Task 4.1** Development of Embedded Distributed Fiber Optic Sensors for Self-sensing Structural Liner (98%), and **Task 4.2** Investigating the Load Transfer between Layers of the CIPP Liner and the Cast-iron Substrate (85%): During this reporting period, the research team (Dr. Ying Huang and Dr. Xingyu Wang) conducted experimental investigations on a pipeline section protected by the smart-liner system. The experiment was designed to enable the smart liner to capture structural deformation and support the development of a corresponding digital twin model. Key findings from this study are summarized below.

(1) Pipe deformation monitoring with smart liner: Compared to the previous study reported in the last quarterly report, which focused on the buckling behavior and impact response of the smart liner system, the current work expands the application by integrating the smart liner into a full-scale pipe

section. The objective is to monitor structural deformation in a liner-protected pipe subjected to mechanical loading. As illustrated in Figure D-11(a), the experimental setup includes an MTS loading machine, a set of embedded sensors, a 3D scanner, and the pipe specimen. To ensure accurate surface capture for 3D modeling, the pipe was sprayed with white paint, enhancing the scanner's ability to detect surface geometry. Figure D-11(b) shows the

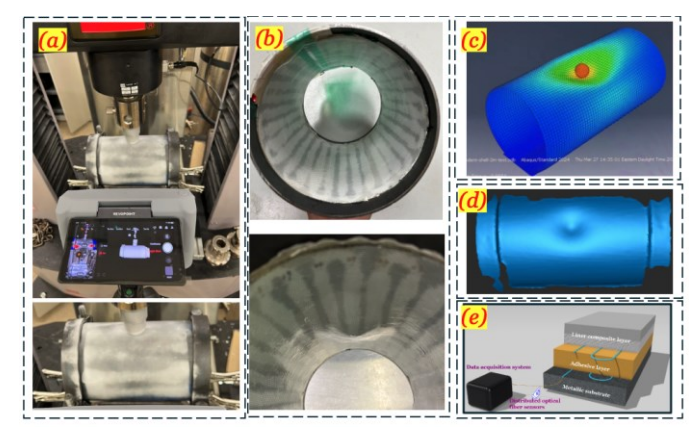


Figure D-11. Pipe sample for dent test.

pipe specimen with the smart liner installed, before and after the dent deformation. Using the load–displacement data acquired from the MTS machine, a finite element analysis (FEA) model was developed and integrated with strain signals obtained from the smart liner's embedded sensors, as depicted in Figure D-11(e). The 3D scan provides a high-resolution reference model used to validate the simulated FEA results, with a focus on the dented region shown in Figure D-11(d). This task is closely coordinated with Task 5.2, which evaluates the structural performance of the smart liner when applied in actual pipe systems.

Task 5.1 Development of CIPP Liner Risk Index for the Pipeline Integrity Management Enhanced by AI Algorithms (75%) and Task 5.2 Full-size laboratory testing for system validation (30%): During this period, the research team (Dr. Chengcheng Tao and Huaixiao Yan, Ph.D. student from Purdue University) conducted assessment activities using datasets generated from the smart-liner-protected pipeline under Task 4. Numerical models were developed for this evaluation and validated against experimental results obtained in Task 4. Key findings are summarized below.

(1) Model Development for Pipe-liner System with Dent Defect: The failure of underground in-service pipes is largely due to localized stress concentrations caused by defects such as dents, which introduce permanent plastic deformation, leading to elevated local strain and cross-sectional ovalization. Figure D-12 shows the experimental and numerical setups. Load–displacement curves from the experiment were compared with FEA results for validation, as shown in Figure D-12(a). Among the tested materials, A513-1035 steel, used in the simulation, showed the best match to experimental data, with a maximum load difference of only 3.9%. Additionally, the model was extended to simulate load–displacement responses for other steel types, including X52 and A513-1010, to build a broader database. These results confirm the reliability of the FEA model in simulating steel pipe behavior under displacement-controlled denting.

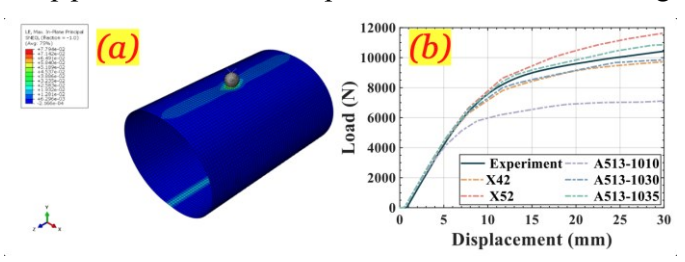


Figure D-12. (a) Finite element model of the steel tubing sample and indenter, (b) comparison of load-displacement curves for the steels under dent test.

(1) Pipe-liner system with dent defect: In order to demonstrate the practical implication of this study, a full-scale pipe model is developed to simulate a full-scale pipeline affected by a dent defect. The length of one segment of the underground pipeline is 3657.6 mm (12 ft). Since the indentation is

applied at the top center of the pipe, a halfsymmetric model is created to simplify the analysis. The indenter used in the simulation is identical in size to that used in the experiment to ensure consistency. Five dent depth ratios are selected for this study: 3 OD, 6 OD, 9 OD, 12 OD, and 15 OD, representing a broad range of potential dent severities encountered in underground pipelines. The estimated cyclic load is uniformly applied on the interior surface on the pipe after indentation, ranging from 5.91 - 11.82 MPa. According to the FEA results, the stress concentration around the dent increases as the dent depth ratio becomes larger. Table D-1 presents the estimated fatigue life as a function of dent depth ratio. The residual dent depth ratio, which is slightly lower than the applied value due to elastic

**Table D-1.** The effect of dent depth ratio on estimated fatigue cycles.

Dent depth	Residue dent	Altering	Estimated
ratio	depth ratio	stress (MPa)	fatigue cycles
3%	1.99%	46.945	731253
6%	4.59%	52.698	75786
9%	7.22%	62.779	17193
12%	9.89%	74.552	5672
15%	12.56%	90.357	2099

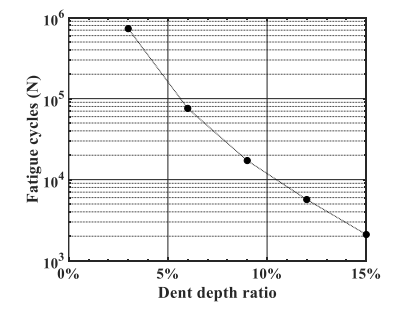


Figure D-13. The fatigue cycles of a dented pipe with different dent depth ratios.

spring-back, is obtained after removing the indenter. As the dent depth increases, a larger portion of the pipe undergoes permanent plastic deformation, resulting in a lower restoration rate. Once the changing stress under cyclic loading is extracted from the simulation, the fatigue cycles can be estimated. At the operating condition, when the dent depth ratio is 3%, the alternating stress is 46.945 MPa, and fatigue cycles can reach up to 731,253 cycles. However, as the dent severity increases, for example, when the dent depth ratio rises from 3% to 6%, the fatigue life decreases by approximately 90%. Further increases in dent depth continue to reduce the fatigue life significantly, resulting in a serious safety risk. Figure D-13 shows the estimated fatigue cycle for different dent depth ratios, providing a practical reference for fatigue life assessment of dented pipes. The findings emphasize the critical importance of dent depth in pipeline fatigue performance

and provide a validated computational approach for estimating fatigue life under operational loading conditions.

# Project Financial Activities Incurred during the Reporting Period:

The cost breakdown during the reporting period according to the budget proposal is shown in Table D-2. Table D-2. Cost breakdown

Tuok B 2. Cost of cardown			
Category	Amount spent during Q12		
Personnel			
Faculty	\$0.00		
Postdoc	\$13,956.94		
Students (RA and UR)	\$14,513.95		
Benefits	\$3,751.88		
Operating Expenses			
Travel	\$2,041.20		
Materials and Supplies	\$1,029.39		
Recharge Center Fee	\$2,652.66		
Consultant Fee	\$1,050.00		
Subcontracts	\$38,080.04		
Indirect Costs	\$18,041.01		

### **Project Activities with Cost Share Partners:**

The Match fund from NDSU for this project is coming from the tuition of the associated graduate students during their work on this project. During the reporting period (Q12), Zahoor Hussain (100%), Austin Knight (100%), and Tofatun Jannet (100%) were working on the project. The tuition for the four students during Q12 was estimated to be \$5,564.76 at a rate of \$463.73 per credit.

### **Project Activities with External Partners:**

During this reporting period, George Ragula, our industry consultant, attended all the bi-weekly meetings with the research team.

#### **Potential Project Risks:**

No potential risks were noticed during this reporting period.

# **Future Project Work:**

The research team will continue working on Tasks 2, 3, 4, and 5.

#### **Potential Impacts on Pipeline Safety:**

Continuing from Q11, a new self-healing formulation was explored to enhance thermal properties. This quarter, the team evaluated formulations incorporating the short-chain aliphatic crosslinker. For the vitrimer system, molecular dynamics simulations were scaled up to achieve a more representative cluster size distribution, along with assessment of glass transition temperature, porosity, and mechanical performance. FEA modeling was also used to analyze the mechanical response and damage behavior in liner-protected substrates. Additionally, the smart-liner system was applied to pipe sections for experimental testing and risk analysis. The results demonstrate the potential applicability of the developed liner system to full-scale pipelines and provide insights for optimizing CIPP liner design and fabrication.